Frequency-Doubled High-Power Optical Vortex Beam With Sub 500 fs Pulse Duration

André Loescher, Christoph Röcker, Florian Bienert, Thomas Graf, and Marwan Abdou Ahmed

***Abstract*—We report on the generation of high-power ultrashort-pulsed optical vortex beams (VBs) with orbital angular momentum (OAM) of $+1$ in the infrared (IR) and $+2$ in the visible (VIS) spectral regions. The IR vortex beam was created from a Gaussian beam by employing a nanograting (S-waveplate) mode converter. With this approach we obtained an average power of up to 802 W at a wavelength of $\lambda = 1030$ nm in the IR-VB with a pulse energy of 802 µJ, a pulse duration of 460 fs, and a mode-conversion efficiency of 90.1%. By subsequent second harmonic generation, the IR-VB was frequency-doubled inside a lithium triborate (LiB_3O_5) crystal. An average power of up to 320 W at $\lambda = 515$ nm was generated, with 320 µJ of pulse energy, 382 fs of pulse duration, and an IR-VB to SH-VB conversion efficiency of 39.9%. The generated IR and VIS VBs were characterized by a Mach-Zehnder type interferometric measurement, confirming the helical wavefronts at these high average powers. These results show that it is possible to efficiently generate high-quality VBs at multi hundreds of watts and confirm the OAM scaling law in harmonic generation processes.**

***Index Terms*—High power ultrafast lasers, optical vortex, second harmonic generation.**

I. Introduction

PARAXIAL beams which exhibit propagating optical vortices are commonly referred to as vortex beams (VBs). Such beams manifest orbital angular momentum (OAM) as proposed in [1]. The Laguerre-Gaussian (LG) modes are one well-known class of these vortex beams since they can carry OAM and are easy to generate in the laboratory [2]. The individual OAM is directly related to the phase term $e^{il\varphi}$ and amounts to $l\hbar$ per photon with l being an integer number, φ the azimuthal angle, and $\hbar$ the Planck constant [1]. Hence, VBs possess a spiral wave front with an azimuthal phase change of $2\pi l$. They exhibit different behavior in reflection, refraction, diffraction, interference, polarization and quantum properties compared to conventional light [3]. VBs are therefore of great interest in several fields of applications such as free-space optical communication [4], microscopy [5], quantum information [6], relativistic and plasma physics [7], [8], and many more. Especially in light-matter interactions such as laser materials processing, it was demonstrated that the OAM of light can be transferred to the workpiece [9], [10]. A chiral surface relief with a height of approx. 1 µm was created in an azo-polymer film [9]. Chiral nanostructures such as nanoneedles with a height of about 10 µm and a tip curvature of about 50 nm were produced in tantalum [10]. Furthermore, chiral nanojets on thin metal films [11], surface structuring [12], or nanochannels in dielectric media [13] were demonstrated using VBs. To drive these applications and processes at higher speeds, lasers, which emit light with these special properties at high average power are required. Since the laser-matter interaction is largely determined by the wavelength of light, different applications benefit from different spectral properties of the incident beam. One potential application is large-area surface structuring using high-power VBs at wavelengths around 515 nm. Due to the specific intensity profile of vortex beams (steeper intensity flanks compared to Gaussian intensity profile) heat accumulation effects are reduced and the quality of the surface structures can be increased. Using laser-induced periodic surface structuring (LIPSS) one can produce structures with a period in the order of the radiation wavelength. It has been demonstrated e.g., by Helbig et al. that the cell adhesion of Staphylococcus epidermidis and Escherichia coli bacteria was suppressed on hole structures with a period of 500 nm compared to the cell adhesion of these bacteria on structures with a periodicity of 1000 nm which is typically achieved with IR beams [14]. VBs at various wavelengths ranging from the ultraviolet up to the mid-infrared have already been demonstrated [15], [16]. Their generation can be achieved directly in a laser cavity or by converters outside the cavity [3]. Spiral phase plates (SPPs) [17], q-plates [5], and spatial light modulators (SLMs) [18] are commonly used as mode-converters from Gaussian beams to VBs. These converters support the conversion of both continuous-wave and pulsed radiation. However, other approaches to create VBs were recently demonstrated. Modulation of transverse modes in a compact two mode fiber laser was used to generate VBs with variable pulse duration in the range of 0.84-5.28 ps at a wavelength of 1547 nm and an average power of around 10 mW [19]. VBs with 740 W of average power with a pulse duration of 390 fs at a repetition rate of 55 MHz at a central wavelength of 1032 nm are reported on in [20]. This system was based on tiled-aperture coherent beam combination where the VBs were generated by individually controlling the phase of each laser channel. Another approach is the interferometric generation of VBs directly inside a resonator [21]. The generation of up to 31 W of average power at a repetition rate of 600 kHz and at a wavelength of 1064 nm was

Manuscript received 29 August 2022; revised 23 November 2022; accepted 24 November 2022. Date of publication 1 December 2022; date of current version 3 April 2023. This work was supported in part by the European Union within the Horizon 2020 framework Programme 825246 (project kW-Flexiburst). This project is an initiative of the Photonics Public Private Partnership from the European Union's Horizon 2020 Research and Innovation Programme under Grant Agreement 825246. *(André Loescher, Christoph Röcker, and Florian Bienert contributed equally to this work.) (Corresponding author: André Loescher.)*

The authors are with the Institut für Strahlwerkzeuge (IFSW), University of Stuttgart, 70569 Stuttgart, Germany (e-mail: andre.loescher@ifsw.uni-stuttgart.de; christoph.roecker@ifsw.uni-stuttgart.de; florian.bienert@ifsw.uni-stuttgart.de; thomas.graf@ifsw.uni-stuttgart.de; marwan.abdou-ahmed@ifsw.uni-stuttgart.de).

Color versions of one or more figures in this article are available at https://doi.org/10.1109/JLT.2022.3225903.

Digital Object Identifier 10.1109/JLT.2022.3225903

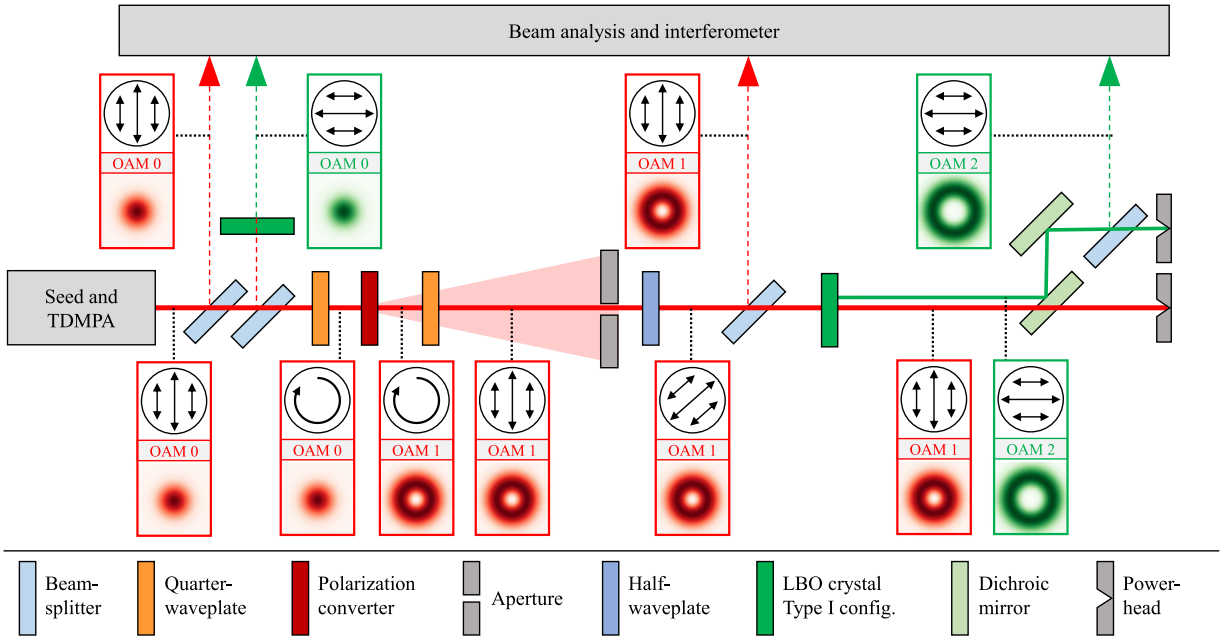

Fig. 1. Simplified sketch of the experimental setup. The linearly polarized IR-beam was converted into a linearly polarized IR-vortex beam by using two QWPs and a polarization converter (S-waveplate). The IR-vortex beam was frequency-doubled using an LBO crystal. Beam splitters were implemented to generate low-power replicas of the pulses for beam analysis. The insets show schematically the transverse mode profile and the arrows indicate the polarization state.

demonstrated in a Q-switched laser with this scheme [22]. Up to 5.7 W of average power at a repetition rate of 24.4 MHz with a compressed pulse duration of 76 fs were demonstrated in a fiber based Mamyshev oscillator [23]. Here, the optical vortex was generated by implementing a q-plate together with quarter-wave plates inside the oscillator. Considering high energy lasers, VBs were generated at the ASTRA laser facility using a spiral phase plate made of polymethyl methacrylate. The incident laser beam on the sample was 50 fs short and had a pulse energy of about 600 mJ at a central wavelength of 800 nm [24]. A different approach was taken in the UHi100 facility, where laser induced fork plasma gratings were used to diffract the laser pulses possessing orbital angular momentum after diffraction [25]. The generation of VB laser pulses at a central wavelength of 800 nm, a pulse duration of 25 fs and a peak power of 100 TW, corresponding to a pulse energy of 2.8 J, at a repetition rate of 10 Hz were shown by this method.

In terms of frequency conversion of VBs, different nonlinear crystals such as beta barium borate (BBO) [26], lithium triborate (LBO) [27], bismuth triborate (BIBO) [28], and MgO-doped periodically poled lithium niobate (MgO:PPLN) [16] were used. Additionally, high harmonic generation (HHG) was demonstrated by tightly focusing optical vortices into an argon gas [29], [30]. Herewith extreme ultraviolet light could be generated with a wavelength of 32.6 nm and 35 nm, respectively.

To date, there is no demonstration and characterization of a powerful beam carrying OAM in the visible spectral region with sub 500 fs pulses and average powers of several hundreds of watts. In this paper, we report the generation and frequency conversion of beams carrying OAM with high average powers. We generated 802 W of average power P_{av} at a wavelength of $\lambda = 1030$ nm and 320 W of average power at $\lambda = 515$ nm with pulse durations τ of less than 500 fs at a repetition rate of f_{rep} 1 MHz.

II. Experimental Setup & Results

The IR-laser that was used for the generation of the vortex beam is presented in detail in Ref. [31]. It comprised of a commercial ultrafast seed laser Spirit-100 from MKS-Spectra Physics and a subsequent Yb:YAG thin-disk multipass amplifier (TDMPA). The pulses of the seed laser ($M^2 < 1.2$, $P_{av} =$ 100 W, $\lambda = 1030$ nm, $f_{rep} = 1$ MHz, $\tau = 260$ fs) were directed into the TDMPA to increase the pulse energy and the average power to 0.9 mJ and 900 W, respectively. At this power level a pulse duration of $\tau = 472$ fs and an $M^2 <$ 1.2 were measured. The two-staged generation of the VB in the visible spectral range (VIS-VB) is schematically shown in Fig. 1. First two low-power replicas of the Gaussian IR beam were created, whereby one of them is frequency doubled with an LBO crystal with a length of 1.7 mm. The crystal was cut for type I (oo-e) phase-matching at 37 °C, which corresponds to angles of $\theta = 90°$, $\phi = 13.6°$. The two replicas served the interferometric analysis. After passing the beam splitters the high-power linearly polarized Gaussian-shaped IR-beam (OAM 0) was used to generate a linearly polarized ring-mode (IR-VB) with OAM +1.

This was achieved by an uncoated S-waveplate [32] made of fused silica which was positioned between two quarter-wave plates (QWPs).The circularly polarized IR-beam after the first QWP was converted into a circularly polarized doughnut-shaped beam using the S-waveplate. The second QWP was used to convert the circular polarization back to linear polarization. Without the QWPs, i.e., when directing the linearly polarized beam directly through the S-waveplate, a vector beam with OAM 0 and radial polarization would be the result [33].

The Infrared Gaussian beam can be frequency-doubled first and subsequently converted into a vortex beam in order to obtain a VIS-VB with OAM of $l = 1$. However, the variety of generating

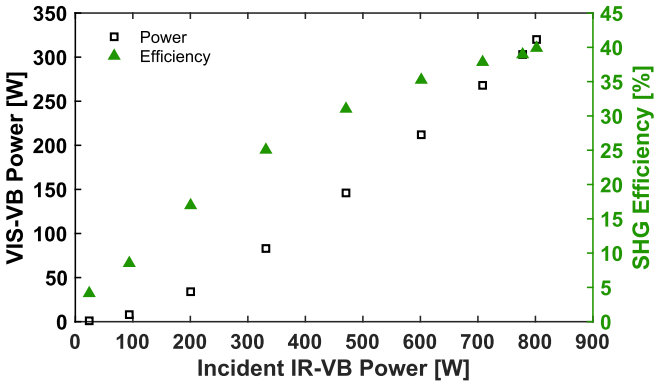

Fig. 2. Power of frequency doubled beam and conversion efficiency as a function of the phase-matched incident IR-power.

different OAM beams is higher by frequency-doubling infrared Gaussian and VBs thanks to the interaction phenomena of VBs in nonlinear crystals [34].

The conversion from a Gaussian beam shape to the ring mode was accompanied by the formation of low-intensity radiation emerging with a large divergence, which was spatially filtered out by a subsequent aperture. After this spatial filter, the IR-VB had a beam propagation factor of $M^2 = \sqrt{M_x^2 \cdot M_y^2} = \sqrt{2.35 \cdot 2.92} = 2.63$ and a remaining power of 802 W, yielding a mode conversion efficiency of 90.1%, whereby about 8% of the losses are related to the Fresnel reflections at the surfaces of the uncoated S-waveplate.

The IR-VB was then directed through a half-wave plate (HWP) into an LBO crystal with the same specifications of the LBO crystal described above. Exploiting the polarization sensitivity of the nonlinear process, the HWP enabled the adjustment of the power for the SH beam by adapting the incident linear polarization of the IR-VB in the LBO crystal. Setting the linear polarization vertical to the optical table (along the crystal's critical plane) second harmonic generation (SHG) was suppressed.

The frequency-doubled and fundamental vortex beams were separated by two dichroic mirrors placed behind the LBO crystal. Using the maximum available IR power of 802 W, 320 W of power was measured at the second harmonic frequency, which corresponds to a frequency conversion efficiency of 39.9%.

Fig. 2 shows the measured second harmonic power and frequency conversion efficiency as a function of the incident IR power with the phase-matched horizontal polarization (perpendicular to the crystal's critical plane).

The phase-matching was optimized at the maximum power by tuning the critical axis to maximize the conversion efficiency. The frequency converted and the fundamental beams were analyzed by means of a commercial beam propagation analyzer (Ophir Photonics Beam Squared), autocorrelators (PulseCheck 150 (TPA for SHG), APE Berlin), and spectrometers (HR4000, Ocean Optics). Fig. 3 shows the beam caustics of the IR- and VIS-beams at maximum power. The insets show the intensity profiles of the corresponding far and near fields. The beam propagation factor was $M^2 = \sqrt{3.07 \cdot 3.74} = 3.39$ at a power of 320 W for the VIS-VB. This is in good agreement with the conservation of momentum where the frequency doubled beam (VIS-VB) requires an OAM of $+2$ [35], which results in energy

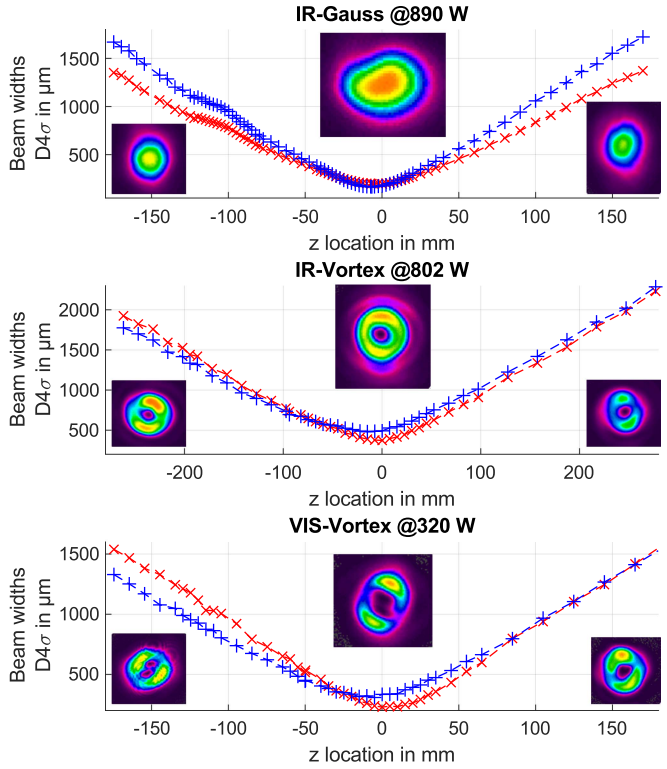

Fig. 3. Measured beam caustics and corresponding near- and far-field intensity profiles of the IR-Gaussian (top), the IR-VB (center), and VIS-VB (bottom) at maximum power.

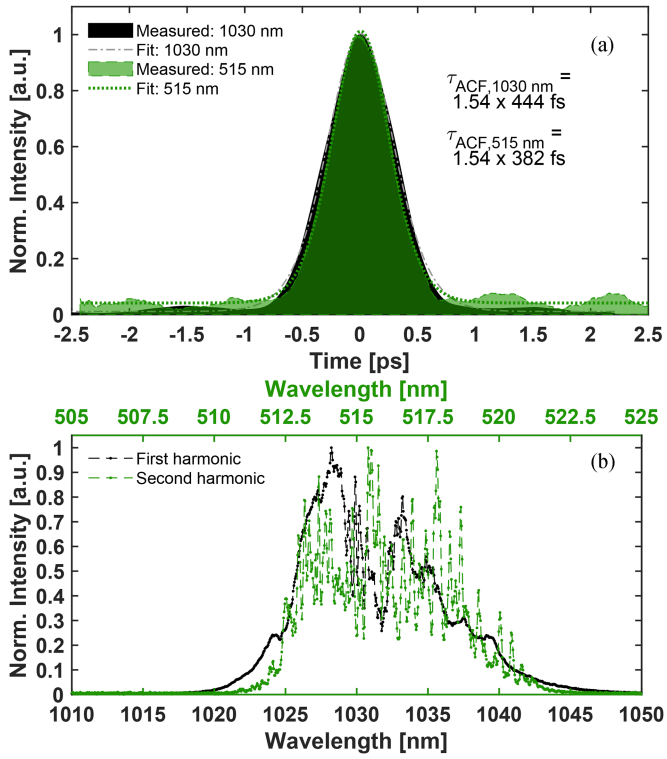

Fig. 4. Measured autocorrelations (a) and spectra (b) of the IR- and VIS-VB at 802 W and 320 W of power, respectively. The spectral resolution of the spectrometer used for the visible spectrum was about a factor of 2 higher.

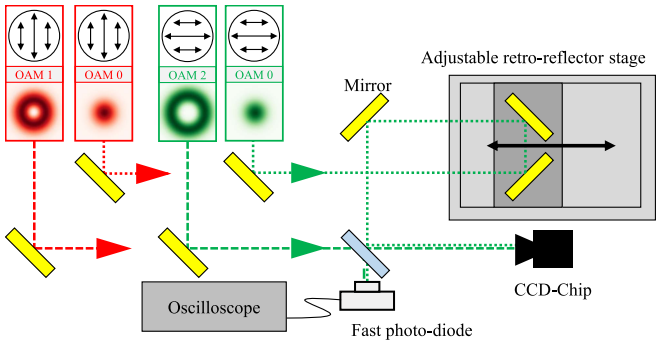

Fig. 5. Schematic of the Mach-Zehnder interferometer. A retro-reflector on a linear translation stage was used to adjust the propagation lengths of the individual beams which were about 7.5 m. The adjustable optical distance (retro-reflector stage) was 100 mm. A fast photodiode behind a beam combiner was used to track the temporal overlap of these low power replicas.

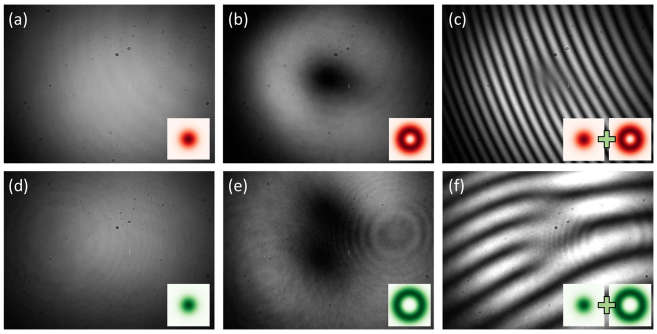

Fig. 6. Experimentally recorded intensity profiles of the low-power replicas. The insets indicate the individual beams: (a)-(c) IR Gaussian beam, IR vortex beam, and IR interference pattern, respectively. (d)-(f) VIS Gaussian beam, VIS Vortex-beam, and VIS interference pattern, respectively.

transfer to a LG02-mode with a theoretical beam propagation factor of M^2=3 [36]. A slight splitting of the singularities of VIS-VB was observed, mainly visible in the far field before the beam waist. This splitting was independent of the generated VIS power and can be attributed to spatial walk-off inside the LBO crystal. This effect was mentioned in the work of Chaitanya [28] and was confirmed by our simulations. The symmetry of the intensity profile is therefore further degraded as compared to the doughnut-shaped intensity profile of the infrared vortex beam. As will be shown later in Fig. 6, the frequency-doubled beam is however a higher-order vortex beam with an azimuthal phase change of 4π.

It is worth noting that a walk-off compensation could be implemented in order to prevent the splitting of the singularities. This can be achieved by using an identical second nonlinear crystal which is oriented in such a way that the spatial walk-off direction is reversed, thus resulting in a total walk-off with zero magnitude. Such a compensation scheme was implemented and demonstrated for harmonic generation using BBO [37], [38]. Fig. 4 shows the measured autocorrelations and spectra of the IR-VB and the VIS-VB. The measured pulse durations were 444 fs for the IR-VB and 382 fs for the VIS-VB assuming a sech^2 temporal shape. The decrease of the pulse duration of the frequency-doubled pulse is a well- known phenomenon related to the intensity-dependence of the nonlinear process. In order to obtain transform-limited pulses at a wavelength of 515 nm (time-bandwidth limit of approx. 56 fs), we estimated that a group delay dispersion of –7600 fs^2 is needed. It is worth mentioning that it is not expected that subsequent pulse compression affects the vortex nature of the beam as it was shown for pulses with similar duration in [39]. This can be subject of further investigations. The OAM of the VBs was verified by a home-built Mach-Zehnder interferometer, as schematically shown in Fig. 5. For the analysis of the VBs OAM, coherent Gaussian replicas are required for each wavelength, i.e., IR and VIS. To generate these, the two above mentioned beam splitters directly behind the TDMPA were used.

While the analysis of the IR-VB was carried out with a low-power replica of the Gaussian beam exiting the amplifier, the analysis of the VIS-VB required additional frequency-doubling of the Gaussian low-power IR replica to obtain a coherent reference beam at the second harmonic wavelength ($\lambda = 515\ nm$) with a Gaussian intensity profile. Therefore, a second LBO crystal with identical specifications, i.e., cut and length, was used for the conversion of the low-power Gaussian IR beam (OAM 0), as depicted in Fig. 1. The low-power replicas of the VBs were then brought to interference with low-power Gaussian replicas (for each wavelength) at the position of the CCD chip of the camera to obtain a high contrast at the location of the phase-singularity. Presence and order of the OAM were verified by the characteristic fork patterns [3]. To ensure the crucial temporal overlap between the Gaussian and Vortex-beam pulses (corresponding to $\sim$100 µm of propagation distance for our pulses), the optical path lengths of several meters were carefully adjusted with a retro-reflecting mirror pair that was mounted on a linear stage to compensate differences in optical length of up to $\sim$100 mm. Fig. 6 shows the recorded intensity patterns of the low-power replicas at maximum power. The first column (Fig. 6(a) and (d)) shows the intensity distribution for the Gaussian IR and VIS beams. The second column (Fig. 6(b) and (e)) presents the intensity profiles of the vortex IR and VIS beams. The resulting interference patterns are shown in the third column for the IR (Fig. 6(c)) and VIS beams (Fig. 6(f)). The fork patterns reveal the vortex orders of $l = 1$ and $l = 2$ for the IR-VB and the VIS-VB, respectively. The high contrast indicates the mutual coherence and mode purity. The line resolution and the orientation of the fork are different, since the alignment of the beam with the infrared pulses was slightly different from the one of the beam with the visible pulses. Furthermore, the patterns differ due to the different phase of the infrared VB and the frequency-doubled VB.

III. Conclusion

We presented the generation of double rotated (OAM 2) vortex pulses with an average power of $P_{av} = 320\ W$, a pulse energy of $E = 0.32\ mJ$ (1 MHz), pulse durations of $\tau = 430\ fs$, and a beam propagation factor of $M^2 = 3.39$ (i.e., close to the theoretical optimum: $M^2 = 3$) in the visible spectral range ($\lambda = 515\ nm$) in a two-stepped process.

First a combination of two QWPs and a S-waveplate was used to convert Gaussian NIR (1030 nm) pulses, amplified by a TDMPA to NIR-vortex pulses with a mode-conversion efficiency of 90.1%. These mode-converted IR pulses with $P_{av} = 802\ W$, $E = 0.8\ mJ$ (1 MHz), and $\tau = 472\ fs$, were subsequently frequency-converted using a 1.7 mm long type I (oo-e) cut LBO-crystal resulting in the described green

vortex beam with OAM 2. The phase fronts and OAMs of both the IR and VIS vortices were analyzed with a home-built Mach-Zehnder interferometer, where the vortices were brought to interference with coherent Gaussian replicas, proving the suitability of the presented method. The excellent beam qualities and the stable operation of the system are encouraging to aim for further output power and conversion into the ultraviolet spectral range.

ACKNOWLEDGMENT

The authors thank Workshop of Photonics for providing the S-waveplate, Cristal Laser for providing the nonlinear crystals, and Spectra-Physics for the seed laser.

REFERENCES

[1] L. Allen, M. W. Beijersbergen, R. J. C. Spreeuw, and J. P. Woerdman, "Orbital angular momentum of light and the transformation of Laguerre-Gaussian laser modes," *Phys. Rev. A*, vol. 45, no. 11, pp. 8185–8189, Jun. 1992.

[2] M. W. Beijersbergen, L. Allen, H. E. L. O. van der Veen, and J. P. Woerdman, "Astigmatic laser mode converters and transfer of orbital angular momentum," *Opt. Commun.*, vol. 96, no. 1–3, pp. 123–132, 1993.

[3] Y. Shen et al., "Optical vortices 30 years on: OAM manipulation from topological charge to multiple singularities," *Light Sci. Appl.*, vol. 8, no. 1, 2019, Art. no. 90.

[4] H. Zhou et al., "Demonstration of turbulence resiliency in a mode-, polarization-, and wavelength-multiplexed free-space optical link using pilot-assisted optoelectronic beam mixing," *J. Lightw. Technol.*, vol. 40, no. 3, pp. 588–596, Feb. 2022.

[5] L. Yan et al., "Q-plate enabled spectrally diverse orbital-angular-momentum conversion for stimulated emission depletion microscopy," *Optica*, vol. 2, no. 10, pp. 900–903, 2015.

[6] A. Mair, A. Vaziri, G. Weihs, and A. Zeilinger, "Entanglement of the orbital angular momentum states of photons," *Nature*, vol. 412, no. 6844, pp. 313–316, 2001.

[7] R. Aboushelbaya et al., "Orbital angular momentum coupling in elastic photon-photon scattering," *Phys. Rev. Lett.*, vol. 123, no. 11, 2019, Art. no. 113604.

[8] J. Vieira, J. T. Mendonça, and F. Quéré, "Optical control of the topology of laser-plasma accelerators," *Phys. Rev. Lett.*, vol. 121, no. 5, Jul. 2018, Art. no. 54801.

[9] M. Watabe, G. Juman, K. Miyamoto, and T. Omatsu, "Light induced conch-shaped relief in an azo-polymer film," *Sci. Rep.*, vol. 4, no. 1, 2014, Art. no. 4281.

[10] K. Toyoda et al., "Transfer of light helicity to nanostructures," *Phys. Rev. Lett.*, vol. 110, no. 14, Apr. 2013, Art. no. 143603.

[11] S. Syubaev et al., "Direct laser printing of chiral plasmonic nanojets by vortex beams," *Opt. Exp.*, vol. 25, no. 9, pp. 10214–10223, 2017.

[12] J. J. J. Nivas et al., "Direct femtosecond laser surface structuring with optical vortex beams generated by a q-plate," *Sci. Rep.*, vol. 5, no. 1, 2015, Art. no. 17929.

[13] C. Hnatovsky, V. G. Shvedov, W. Krolikowski, and A. V. Rode, "Materials processing with a tightly focused femtosecond laser vortex pulse," *Opt. Lett.*, vol. 35, no. 20, pp. 3417–3419, Oct. 2010.

[14] R. Helbig, D. Günther, J. Friedrichs, F. Rößler, A. Lasagni, and C. Werner, "The impact of structure dimensions on initial bacterial adhesion," *Biomater. Sci.*, vol. 4, no. 7, pp. 1074–1078, 2016.

[15] T. Omatsu, K. Miyamoto, and A. J. Lee, "Wavelength-versatile optical vortex lasers," *J. Opt.*, vol. 19, no. 12, 2017, Art. no. 123002.

[16] V. Sharma, S. C. Kumar, G. K. Samanta, and M. Ebrahim-Zadeh, "Tunable, high-power, high-order optical vortex beam generation in the mid-infrared," *Opt. Exp.*, vol. 30, no. 2, pp. 1195–1204, Jan. 2022.

[17] S. S. R. Oemrawsingh, E. R. Eliel, J. P. Woerdman, E. J. K. Verstegen, J. G. Kloosterboer, and G. W. 'T. Hooft, "Half-integral spiral phase plates for optical wavelengths," *J. Opt. A: Pure Appl. Opt.*, vol. 6, no. 5, 2004, Art. no. S288.

[18] N. R. Heckenberg, R. McDuff, C. P. Smith, and A. G. White, "Generation of optical phase singularities by computer-generated holograms," *Opt. Lett.*, vol. 17, no. 3, pp. 221–223, 1992.

[19] D. Mao et al., "Optical vortex fiber laser based on modulation of transverse modes in two mode fiber," *APL Photon.*, vol. 4, no. 6, 2019, Art. no. 60801.

[20] M. Veinhard et al., "Orbital angular momentum beams generation from 61 channels coherent beam combining femtosecond digital laser," *Opt. Lett.*, vol. 46, no. 1, pp. 25–28, Jan. 2021.

[21] D. N. Naik, N. A. Saad, D. N. Rao, and N. K. Viswanathan, "Ultrashort vortex from a Gaussian pulse—An achromatic-interferometric approach," *Sci. Rep.*, vol. 7, no. 1, pp. 1–10, 2017.

[22] J. W. T. Geberbauer, W. R. Kerridge-Johns, and M. J. Damzen, " >30 W vortex LG 01 or HG 10 laser using a mode transforming output coupler," *Opt. Exp.*, vol. 29, no. 18, pp. 29082–29094, 2021.

[23] D. Lin, Y. Feng, Z. Ren, and D. J. Richardson, "The generation of femtosecond optical vortex beams with megawatt powers directly from a fiber based Mamyshev oscillator," *Nanophotonics*, vol. 11, no. 4, pp. 847–854, 2022.

[24] R. Aboushelbaya et al., "Measuring the orbital angular momentum of high-power laser pulses," *Phys. Plasmas*, vol. 27, no. 5, May 2020, Art. no. 053107.

[25] A. Leblanc, A. Denoeud, L. Chopineau, G. Mennerat, P. Martin, and F. Quéré, "Plasma holograms for ultrahigh-intensity optics," *Nature Phys.*, vol. 13, no. 5, pp. 440–443, 2017.

[26] G. Gui, N. J. Brooks, H. C. Kapteyn, M. M. Murnane, and C. T. Liao, "Second-harmonic generation and the conservation of spatiotemporal orbital angular momentum of light," *Nature Photon.*, vol. 15, no. 8, pp. 608–613, 2021.

[27] A. Abulikemu, T. Yusufu, R. Mamuti, S. Araki, K. Miyamoto, and T. Omatsu, "Octave-band tunable optical vortex parametric oscillator," *Opt. Exp.*, vol. 24, no. 14, pp. 15204–15211, Jul. 2016.

[28] N. A. Chaitanya, A. Aadhi, M. V. Jabir, and G. K. Samanta, "Frequency-doubling characteristics of high-power, ultrafast vortex beams," *Opt. Lett.*, vol. 40, no. 11, pp. 2614–2617, Jun. 2015.

[29] A. de las Heras et al., "Extreme-ultraviolet vector-vortex beams from high harmonic generation," *Optica*, vol. 9, no. 1, pp. 71–79, 2022.

[30] L. Rego et al., "Generation of extreme-ultraviolet beams with time-varying orbital angular momentum," *Science*, vol. 364, no. 6447, Jun. 2019, Art. no. eaaw9486.

[31] A. Loescher et al., "Thin-disk multipass amplifier delivering sub-400 fs pulses with excellent beam quality at an average power of 1 kW," *Opt. Continuum*, vol. 1, no. 4, pp. 747–758, Apr. 2022.

[32] M. Beresna, M. Gecevičius, P. G. Kazansky, and T. Gertus, "Radially polarized optical vortex converter created by femtosecond laser nanostructuring of glass," *Appl. Phys. Lett.*, vol. 98, no. 20, 2011, Art. no. 201101.

[33] M. A. Ahmed et al., "High-power thin-disk lasers emitting beams with axially-symmetric polarizations," *Nanophotonics*, vol. 11, no. 4, pp. 835–846, 2022.

[34] A. Beržanskis, A. Matijošius, A. Piskarskas, V. Smilgevičius, and A. Stabinis, "Sum-frequency mixing of optical vortices in nonlinear crystals," *Opt. Commun.*, vol. 150, no. 1–6, pp. 372–380, 1998.

[35] K. Dholakia, N. B. Simpson, M. J. Padgett, and L. Allen, "Second-harmonic generation and the orbital angular momentum of light," *Phys. Rev. A*, vol. 54, no. 5, pp. R3742–R3745, Nov. 1996.

[36] R. L. Phillips and L. C. Andrews, "Spot size and divergence for Laguerre Gaussian beams of any order," *Appl. Opt.*, vol. 22, no. 5, pp. 643–644, 1983.

[37] M. V. Pack, D. J. Armstrong, A. V. Smith, and M. E. Amiet, "Second harmonic generation with focused beams in a pair of walkoff-compensating crystals," *Opt. Commun.*, vol. 221, no. 1–3, pp. 211–221, 2003.

[38] Y. Sasaki et al., "Ultraviolet vortex generation using periodically bonded β-BaB_2O_4 device," *Opt. Exp.*, vol. 22, no. 11, pp. 12829–12835, Jun. 2014.

[39] B.-H. Chen, H.-W. Huang, R.-S. Ye, C.-H. Lu, K. Chen, and S.-D. Yang, "Vortex beam assisted energy up-scaling for multiple-plate compression with a single spiral phase plate," *Opt. Lett.*, vol. 47, no. 17, pp. 4423–4426, Sep. 2022.